Microfluid Nanofluid (2015) 19:1349–1361
DOI 10.1007/s10404-015-1650-9

RESEARCH PAPER

Digital microfluidics chip with integrated intra-droplet magnetic bead manipulation

L. Chen[1] · **R. B. Fair**[1]

Received: 29 June 2015 / Accepted: 10 September 2015 / Published online: 24 September 2015

Abstract This paper demonstrates an integrated device combining both EWD droplet actuation and intra-droplet magnetic bead manipulation. Magnetic bead manipulation is achieved by using current-carrying wires acting as microelectromagnets. The current wire structure is capable of segregating and separating magnetic beads within a droplet. By adjusting the amount of current in the wire structure, high segregation efficiency within the droplet is shown and the separation of two kinds of beads is realized within a distance of 65 μm. The EWD droplet actuation function and the magnetic bead separation function can be operated independently, which provides flexibility when designing operation protocols. The current wire structure is embedded in an EWD electrode without affecting droplet actuation. The vertical structure of the device and its fabrication process are also the same as a normal EWD device. Magnetic bead segregation efficiency of 96.8 % was achieved for 2.8-μm beads that were collected over a distance of 65 μm during a 20-s current pulse. Droplet splitting is shown to allow complete separation of beads into one of the two daughter droplets. And, intra-droplet separation of 1- and 2.8-μm beads was demonstrated over an average distance of 65 μm. This experiment shows the feasibility of performing separation in droplets with a complex mixture of multiple beads, each having different magnetic contents.

Keywords EWOD · Magnetic beads · Droplet · Separation · Velocity

✉ L. Chen
li.ji.chen@duke.edu

[1] Department of Electrical and Computer Engineering, Duke University, Durham, NC 27708, USA

1 Introduction

Electrowetting-on-dielectric (EWD) droplet actuation has been used widely in handling liquid in small quantities in many biological applications (Fair et al. 2007; Miller and Wheeler 2009; Boles et al. 2011; Welch et al. 2011). The droplet is manipulated by applying voltage to EWD electrodes buried beneath an insulator (Fair et al. 2007; Boles et al. 2011; Welch et al. 2011). Many droplet functions have been studied over the years, and those functions include the dispensing, actuation, merging and splitting of droplets (Walker et al. 2009). Different droplet handling functions can be combined and used repeatedly. Those functions can be used together to achieve certain droplet manipulation sequences. Hence, EWD enables the handling of liquid to be programmable and reconfigurable (Fair 2007). These characteristics make EWD technology particularly suitable for integrated systems. To design a complete system for biological applications, it is required to have more than just liquid handling functions. One such function is magnetic actuation, which is used to manipulate magnetic bead for protocols such as molecular separation for purification. Magnetic beads, especially superparamagnetic beads, have been widely used in biological applications. The size of magnetic beads used in such applications is typically in the micrometre to nanometre range, and beads are used to separate molecules from a mixture of biological samples (Alexiou et al. 2006; Cho et al. 2007b; Mach et al. 2013). In such applications, the magnetic beads' surface is modified to allow for binding to specific molecules.

After target molecules have attached to the beads, the beads will then be placed in a high magnetic field gradient environment and be trapped together with the bound molecules. Washing is then applied to the magnetic beads. After

elution, the target molecules may be extracted from the mixture. Such techniques have been used commercially to separate cells from blood and to separate target DNA from complex samples (Gupta and Gupta 2005; Gijs et al. 2010; Mach et al. 2013). In order to incorporate a magnetic function into a microfluidic chip, a permanent magnet has been used in many systems (Wognum et al. 2003; Pamme and Wilhelm 2006; Cho et al. 2007b; Sista et al. 2008; Shah et al. 2010; Berry et al. 2011; Arya et al. 2013). The permanent magnet used in such systems is usually controlled by a mechanical device, and the magnetic field and field gradient are modulated by the location of the magnet (He et al. 2014). By moving the magnet closer to the chip, the magnetic beads will be trapped at the location of the highest magnetic field (Shah et al. 2010). Subsequently, fluidic functions may be conducted, and the beads may be washed for use in subsequent steps. Permanent magnets can have strong magnetic fields and field gradients; as a result, they are capable of trapping large quantities of beads and holding those beads while the next fluidic function is conducted. The magnetic beads can be snapped out of a droplet due to the large magnetic force generated by a permanent magnet (Zhang and Wang 2013). On the other hand, permanent magnets are less successful in separating magnetic beads with small magnetic moment differences.

To solve this issue, several systems have been developed using the combination of an external magnetic field and an on-chip micromagnet to create a changing magnetic field. Such systems can be used to separate magnetic beads with small magnetic moment differences (Yellen et al. 2007; Gao et al. 2010). The equipment needed to generate the external magnetic field is usually very large compared to the size of the required on-chip field, and an on-chip micromagnet can make the fabrication process complicated. As a result, it is difficult for such systems to be integrated with EWD functions to form a compact system. To tackle the challenges of having a compact and integrated system while being able to differentiate two kinds of magnetic beads, the current wire method was found to be more suitable for such requirements. Previously, systems have been reported using current-carrying wires to trap and move magnetic beads (Lee et al. 2004; Wirix-Speetjens and Boeck 2004). Such systems can control the magnetic field more precisely, since the magnetic field is generated by small current-carrying wires, and the resulting field's dimensions are much smaller than those of a permanent magnet. However, there have been no devices reported that integrate a current wire system with EWD functions, other than a short article describing our initial results (Chen et al. 2014). Most of the systems discussed above are directed towards continuous-flow systems. In order to incorporate an intra-droplet particle manipulation and separation capability into an EWD chip, an electrostatic method has been reported in which a weak electric field acts on charged beads with different size and charge (Sung Kwon and Chang-Jin 2003; Cho et al. 2007a). Such a method is not suitable for separating magnetic beads due to the neutral charge characteristics of the beads.

The goal of this paper is to demonstrate an EWD device with integrated magnetic bead separation. A current wire method is adopted, since permanent magnets require a mechanical control system and the magnetic beads' control resolution is limited by the physical size of the permanent magnet. Compared to the permanent magnet method, the current wire method is more ideal, since its wire dimensions are much smaller. The superior control resolution and elimination of mechanical control make integration easier. The current wire method shown in previous studies (Lee et al. 2001) required a cooling system due to the relatively large currents used. However, proper integration should require a limited amount of external support systems for cooling and control. The EWD device should also be able to operate normally without interference from the current wire field generation. This independence is particularly important, since simultaneous droplet actuation and magnetic bead separation should be possible in any biochemical protocol run on the chip. Also the fabrication process of the system should remain simple and should not introduce additional steps. The magnetic function should also be able to perform separation of two kinds of magnetic beads, which is useful in multiple situations. For instance, in cell biology, the separation of beads in different size can be used to sort mixture of cells, thus enabling certain subtype of cells to be manipulated or identified without interference from other cell types. In molecular analysis, different sized magnetic beads can be used to label different molecules and those molecules can be processed at once. Other potential application including focusing the fluorescent labelled bio-samples into a small area and this could be used as an enhancement of the signal.

The basic theory regarding the EWD function and the electromagnet used in the device is discussed in the theory section along with a simplified method to calculate the magnetic field and field gradient generated by the current wire structure. The methods section discusses the design, fabrication and experimental set-up of the system. This paper describes three experiments to illustrate the potential of the device. The results section shows the device can operate properly both as a droplet actuator and as a magnetic bead separator. Also, the device only requires an additional current control supporting system, and it is capable of separating at least two sizes of magnetic beads.

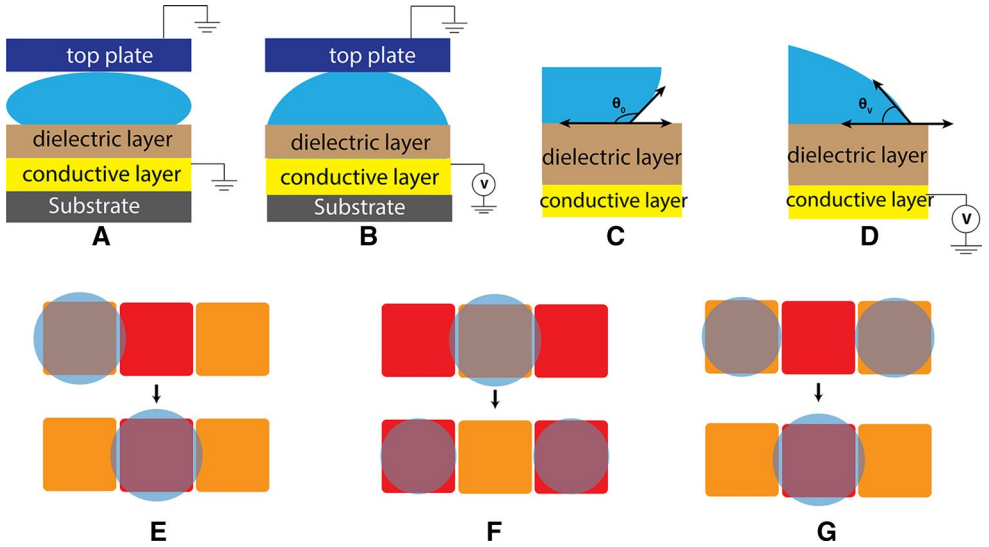

Fig. 1 *A* EWD structure with droplet between the top and bottom plates. *B*: EWD structure with droplet and voltage applied to the electrode. *C* Contact angle between droplet and surface without voltage. *D* Contact angle between droplet and surface with applied voltage. *E* Actuation of droplet. The electrode labelled by *red colour* means voltage has been applied to that electrode. The electrode labelled in *orange* indicates the electrode is grounded. The droplet will move to the location where the electrode has been turned on. *F* Splitting of the droplet. The voltage is applied to the adjacent electrodes, and the droplet is split in half. *G* By applying voltage to the middle electrode, the two droplets on each side are merged together onto the middle electrode (colour figure online)

2 Theory

In this section, two topics will be discussed: the theory behind electrowetting on dielectric (EWD) and the theory behind magnetic bead manipulation. EWD actuation of droplets is the liquid handling technology used in the device and experiments. The theory behind the magnetic bead manipulation is based on the Biot–Savart law (Grant and Phillips 2008), where the magnetic field and magnetic field gradient are generated by currents passing through selected parallel wires (Hiptmair 2002; Jones 2013). Both the EWD function and magnetic function are integrated into the device; hence, it is important to understand the theory behind these two functions.

2.1 Operation of an EWD device

The theory of EWD actuation has previously been reviewed (Mugele and Baret 2005; Fair 2007). An EWD device is realized by applying a voltage difference across an insulator separating a droplet and an electrode. By having multiple electrodes on one device and applying voltages to electrodes in certain sequences, the droplets can be transported, merged and split. The basic structure of the device is shown in Fig. 1A. The system consists of both the top plate and the bottom plate, and a droplet is sandwiched in between. On the bottom plate, the conductive layer is placed on an insulating substrate and a dielectric layer is applied over the conductive layer. The top plate is usually grounded during operation. Both surfaces of top and bottom plates are modified to be hydrophobic. When a voltage is applied to an electrode, the contact angle of the droplet on the dielectric surface is changed. As we can see from Fig. 1B, the applied voltage will make the contact angle of the droplet decrease, thus increasing the wetting area of the droplet. The contact angle between the droplet and surface is θ_0 without supplied voltage. After the voltage has been added to the electrode, the contact angle decreases to θ, as shown in Fig. 1C, D.

By changing the contact angle of the droplet, the droplet can be moved, split and merged as shown in Fig. 1E–G. Actuation of the droplet is achieved by applying voltage to an electrode, which is adjacent to the droplet's location. The droplet will then be moved to a position above the activated electrode. For splitting the droplet, both electrodes on either side of the droplet are activated and the droplet is stretched and split. The two smaller daughter droplets then reside at locations adjacent to the original electrode. The merging function is the reverse action of splitting. By activating the middle electrode, two droplets will be moved and merged on the middle electrode. In this paper, the dispensing, actuation and splitting actions of droplets are used.

2.2 Theory for current wire method

The manipulation of magnetic beads inside a droplet is realized by selectively passing current through parallel wires beneath the droplet. The structure is designed based

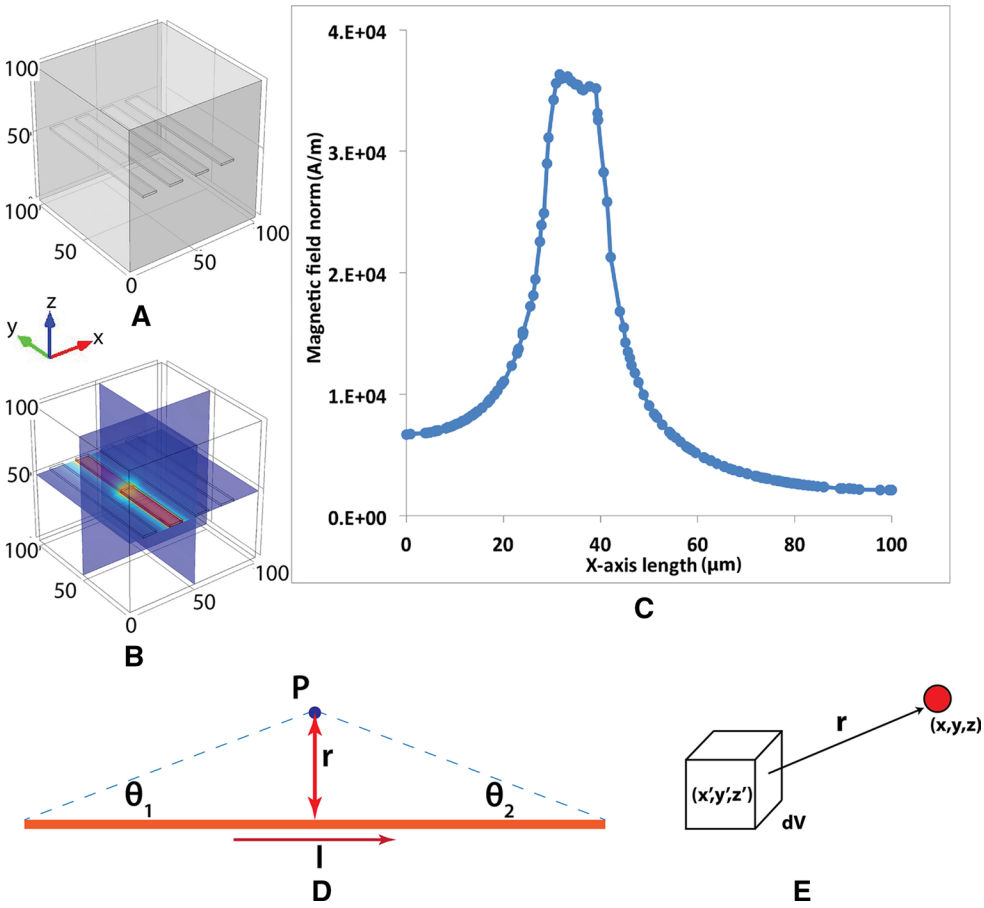

Fig. 2 *A* Four current wires are placed in parallel; this is the basic structure of the device. *B* Current is passed through the second wire counting from the *left*; the magnetic field is shown in *colour*. The magnetic field is higher around the wire that carries the current. *C* Magnetic field along the *x*-axis 2 μm above the wire. *D* Point *P* in space away from wire with distance *r*. The wire has current I passing through it. *E* Small volume *dV* as the source of the magnetic field has coordinates (x', y', z'). A point in space with coordinates (x, y, z) is a distance *r* away from a small *dV* (colour figure online)

on the Biot–Savart law. By passing current in a wire, the magnetic field is generated around the wire. A magnetic field gradient is also created along the direction perpendicular to the wire. The magnetic field gradient generates a magnetic force. Thus if parallel wires run beneath a droplet containing magnetic beads, the magnetic field gradient creates a force that acts on the beads, which are attracted to the location of the peak of the magnetic field.

As shown in Fig. 2, the wire is the basic structure of the device. Several current wires are placed in parallel as shown in part A. In B, the current is passed through the second wire in the *y* direction. The peak of magnetic field is shown in the red colour. The magnetic field shown in part C is calculated 2 μm above the wire in the *z* direction, and the magnetic field is determined on the *x*-axis. It can be seen from part C that the magnetic field gradient is created along the *x*-axis.

The Biot–Savart law is used for calculating the resultant magnetic field *B* at a position *r* generated by a steady current in a wire:

$$B = \frac{\mu_0}{4\pi} \int \frac{J(v) \times \vec{r}}{r^2} dV \tag{1}$$

where $J(v)$ is the current density in the wire given by

$$J(V) = \left[J\left(x'\right), J\left(y'\right), J(z)'\right] \tag{2}$$

And position *r* is calculated as:

$$\vec{r} = \frac{(x - x')i + (y - y')j + (z - z')k}{\left[(x - x')^2 + (y - y')^2 + (z - z')^2\right]^{1/2}} \tag{3}$$

The *dV* in Eq. (1) is the differential element of the structure, which carries the current. In this element, the charge flow remains constant during the time period of concern. The location of the element is labelled as (x', y', z'), and the point in space where the magnetic field is evaluated is labelled as (x, y, z) as shown in Fig. 2E. The displacement between the two points is *r*, and $\vec{r}$ is the unit vector of *r*. The unit vector is calculated by Eq. (3). The term $J(V)$ represents the current density in the small volume *dV* of the structure. By integrating all the elements of the structure, which carry the current, the magnetic field at a point in space can be calculated. By taking the derivative of Eq. (1), the magnetic field gradient can be calculated, which is necessary for the calculation of the magnetic force exerted on the magnetic beads in an adjacent droplet.

The structure of the magnetic wire is a straight metal segment. To simplify the calculation of magnetic force, the formula for magnetic field gradient in the current wire structure is discussed below. As can been seen from Fig. 2D, the current in the wire is I, the distance between the point in space and the wire is r, the angle between the wire and angles formed by the point in space and the ends of the wire is labelled as θ_1 and θ_2. Those parameters are used in calculating the magnetic field at point *P*. The only direction magnetic beads will move is the *x* direction; hence, the magnetic field gradient in the *x* direction is the focus of the following analysis. The simplified expression for the magnetic field of a current wire structure is:

$$B(p) = \frac{\mu_0 I}{4 * \pi * r}(\cos\theta_1 + \cos\theta_2) \tag{4}$$

By using this equation, the magnetic field at certain location of a magnetic bead in a 2D plane can be calculated. The magnetic field gradient is used to calculate the magnetic force exerted on the magnetic bead. By taking the derivative of both sides of Eq. 4, the following expression results:

$$\frac{\mathrm{d}B(p,i)}{\mathrm{d}r} = \frac{-\mu_0 I}{4 * \pi * r^2}(\cos\theta_1 + \cos\theta_2) \tag{5}$$

This result is used to calculate the magnetic force in the *x*-axis, which becomes

$$F = \mu * \frac{-\mu_0 I}{4 * \pi * r^2}(\cos\theta_1 + \cos\theta_2) \tag{6}$$

where μ is the magnetic moment of the bead. The magnetic moment of a bead depends on several factors: the magnetic content inside the bead, the magnetization of the magnetic content and the external magnetic field. The magnetization in the presence of a magnetic field can be determined from previous studies (Fonnum et al. 2005). Based on the magnetization, the magnetic moment can be calculated by multiplying the mass of the magnetic content and the magnetization.

$$m_{\text{beads}} = M_{\text{beads}} \rho V \tag{7}$$

$$F = m_{\text{beads}} * \Delta B \tag{8}$$

The resulting force is used to actuate the magnetic beads inside a droplet. From Eq. (8), the beads' velocity can be estimated and the total time for the beads to travel a certain distance can also be calculated. As an example, if a magnetic force is exerted on beads with the same magnetization characteristic as described in Fonnum et al. (2005) of 1.8 A^2/kg, and the magnetic bead is 10 μm away from an infinitely long wire carrying 200 mA, then multiplying the density of the magnetic content, the magnetic content percentage and the volume of the bead, the magnetic force is calculated to be 2.3 × 10–12 N. From this calculation, the magnetic force required by the system determines the required current in the wires. The current is not the only parameter which has impact on the magnetic field generated. There are other factors, which will influence the magnetic field, which will be discussed next in the methods section.

3 Methods

In this section, the design, fabrication and experimental details will be discussed. The detailed design of the device will be discussed first.

3.1 Design

Three design requirements are central. The first requirement is that the device has two main functions: EWD droplet actuation and magnetic bead manipulation. The second requirement is that both functions must operate simultaneously without interference. The third requirement is that the fabrication process is no more complex than the normal EWD fabrication process. Each function requires specific design elements. Magnetic bead manipulation is realized by a current wire structure, while the EWD droplet actuation requires EWD electrodes. Both design elements are discussed, and then, the combined structure is shown.

The wire structure is designed specifically for the magnetic function; hence, certain design optimization is required to maximize the magnetic field gradient and the magnetic force generated by the structure. The wire structure geometry, the current and the current density are the parameters included in design optimization.

The first thing to consider is the wire array geometry. It can be seen from Fig. 3A that the wire width and thickness determine the cross-sectional area. The wire spacing is important since it has significant impact on the bead velocity during actuation. To determine the design of the wire geometry, the effect of different geometries was studied under a constant current condition. In Fig. 3B, the relationship between the wire geometry and resulting magnetic field is simulated. Three results are shown in the figure. All three simulations used the same wire cross section of 15 μm^2. The first case has wire width of 10 μm and wire thickness of 1.5 μm. The second and third cases have wire widths of 15 and 18.75 μm, respectively, and the respective wire thicknesses were 1 and 0.8 μm. It is clearly shown in the figure that the magnetic field is highest in the first case. The trend is obvious that the narrower and thicker the wire, the higher the magnetic field, assuming the same current density and the same cross-sectional area. The current used in the simulation was 200 mA, which is within the range of current used in the experiments.

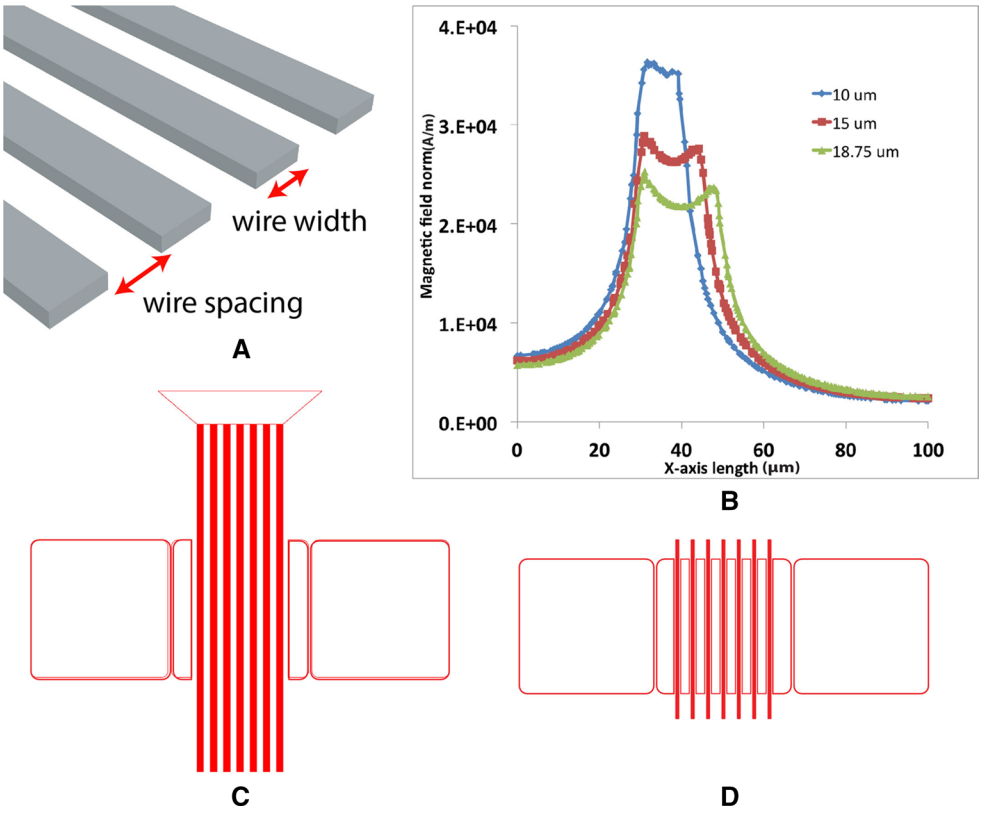

Fig. 3 *A* Geometry of the current wires and wire spacing. *B* Magnetic field with three different wire structures with the same current density and current. *C* Detailed structure of the electrode with space in the middle of the electrode exclusively for the integrated current wires. The *solid red rectangles* are the current wires. *D* Detailed structure of an electrowetting electrode with integrated current wire with interspersed electrode area. The width of the electrode is 700 μm (colour figure online)

The shape of a normal EWD electrode is a square with rounded corners. The area of the electrode combined with the channel height is used to define the droplet volume. The new device has been chosen to have the same electrode area as a normal electrode.

The detailed structure is shown in Fig. 3C, D. The current wires shown in solid red extend out of the entire length of the electrode area to ensure the magnetic beads experience the same force regardless of location inside of the droplet. As a result, the current wires are three times the electrode length. The first device configuration is shown in Fig. 3C. In this case, the narrow EWD electrodes on both sides of the wire array are used to facilitate droplet actuation and are used to define the area of the EWD electrode, so that the device functions the same as the rest of the normal EWD electrodes. Thus, the narrow current wire area has no electrode surface exposed between the wires. During EWD actuation, voltages are applied to the current wires as well as the electrode. The device in Fig. 3D shows the second kind configuration with EWD electrode fingers interspersed between the current wires. Those fingers are shown between the solid red rectangles representing the current wires. By applying voltage to current wires when a droplet is actuated on and off the electrode, the EWD actuation is facilitated, since the device has more area for actuation. Thus, all the wires will have the electrode voltage applied during EWD. In both designs shown in Fig. 3C, D, each current wire can be addressed individually and each electrode can be addressed individually as well.

Based on simulations and fabrication requirements, a wire thickness of 1 μm was used and wire width was 10 or 15 μm. Both the wire thickness and the width are limited by the fabrication capability and the resolution of the mask that are accessible to the author. The performance can be further enhanced, provided the fabrication capability allows the wire to be narrower and taller. The wire spacing was determined by the required effective range of the magnetic force on the magnetic beads. To determine the effective range, the criteria are chosen to have the smaller 1-μm magnetic beads across the spacing under 30 s. Using the formula developed in the theory section, the maximum wire spacing in the device was determined to be 65 μm, which is within the effective range for 1-μm magnetic bead actuation with 150 mA wire current. Spacing between a current wire finger and the adjacent electrode area was 10 μm. The wire spacing includes the finger width between the current wires.

The entire chip layout is shown in Fig. 4A. The chip consisted of two reservoirs separated by a string of electrodes. One current wire electrode is placed in the middle of the string. The EWD electrodes are square-shaped in the metal layer with interconnecting lines to the connection pads. The interconnection lines had width in the range of 10–20 μm. The width was chosen to minimize the EWD effect on the

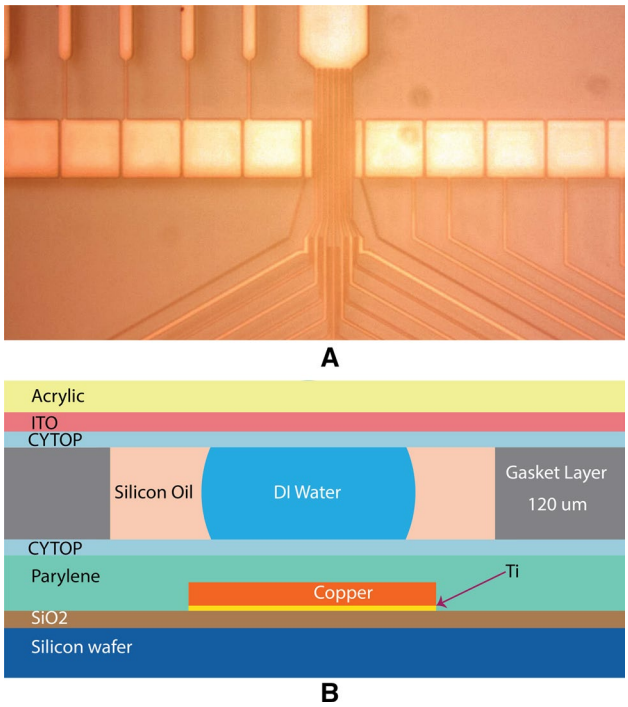

Fig. 4 *A* Entire chip structure. *B* Vertical layer structure of the device

area outside the EWD electrodes. The gap between two electrodes was within the range of 10–40 μm for different designs. Such spacing ensures the droplet can be actuated onto the next electrode. The chip shown in Fig. 4A has square-shaped electrode whose length is 700 μm, while the gap between electrodes is 40 μm.

The layout of the chip determined the experimental procedure. A droplet containing magnetic beads was first dispensed from a reservoir. It was then actuated across the string of electrodes and onto the electrode with integrated current wires. Magnetic bead manipulation within the droplet was then performed; the manipulation included bead separation and segregation. The chip then performed droplet splitting. The resulting droplets were moved, collected and examined for further applications. The detailed experimental procedures will be discussed in the experiment section.

During magnetic bead manipulation, the current density inside the current wire can be as high as 3×106 A/cm^2. Under such high current density, two phenomena need to be considered: the heat generated by the current and the electromigration effect. The heat generated by the current can heat up the surrounding areas and the wire can be damaged due to the rising temperature. Electromigration under high current density can also result in open-circuited wires. To overcome these problems, the material chosen for the current wire structure was copper, since it has low resistivity for less Joule heating and long MTTF (mean time to failure) under high current density. According to the literature (Tao et al. 1993), the MTTF of copper at a current density of 1.5×107 A/cm^2 at room temperature is more than 1×105 h. The MTTF under designed maximum current density is much longer than the required lifetime of the device.

3.2 Fabrication

The vertical structure of the device is shown in Fig. 4B. The bottom plate, the top plate and the gasket were used to form the EWD device. The bottom substrate was a silicon wafer with thickness of 450 μm. A 1-μm-thick layer of thermal oxide was grown on top of the silicon wafer by the wafer supplier and was used to provide a smooth and adhesive base for the metal layer. The fabrication process started with the metal layer deposition. The Ti/Cu stack layer was deposited onto the substrate using an E-beam metal evaporator. The Cu and Ti each had a thickness of 1 μm and 10 nm, respectively. The metal layer was then patterned using lithography and wet-etched into both EWD electrodes and current wires. Due to the thickness of the metal layer, undercutting was especially monitored so that the narrow connection wire stayed intact during the wet etching process. The EWD insulator layer was deposited over the metal layer to provide insulation between the droplet and the metal. The material used for the dielectric layer was either SU-8 or parylene C. For the device using SU-8, the material was spun on and its thickness was controlled to be 2 μm. The thickness of the parylene C was also 2 μm, and it is deposited by vacuum deposition. The thickness of the insulation layer was determined by simulation to have the largest magnetic force while keeping the insulation layer reliable, since a thinner dielectric layer may be more prone to being damaged by high voltage on the electrodes. The CYTOP layer was also spun on and its thickness was 80 nm; hence, the surface in contact with water was hydrophobic. The CYTOP layer completed the bottom plate.

The top plate consisted of three layers. The first layer was based on an acrylic plate, which provided the mechanical support and also acted as observation window, since it is transparent. A 150-nm-think layer of ITO was sputtered onto the acrylic plate to provide ground connection during experiments. During operation, the top plate was grounded at all times. CYTOP was spun onto the top plate with thickness of 80 nm. The CYTOP material also reduced the adhesive effect between the magnetic beads and the dielectric surface. The 120-μm-thick SecureSeal sheet was cut by a laser machine to be the gasket layer defining the channels in which all the experiments are conducted. The top and bottom plates were bonded together by the double-sided adhesive gasket layer.

3.3 Experiment

3.3.1 Magnetic beads and liquids

The magnetic beads chosen for the experiment were Dynabeads® M-270 and MyOne. The magnetic beads are chosen due to their uniformity both in size and the magnetic content as well as the lack of aggregation. The M-270 beads and the MyOne magnetic beads have diameters of 2.8 and 1 μm, respectively. The size distribution CV of M-270 is less than 3 % according to the manufactory; the size distribution CV of MyOne magnetic bead is <5 %. There is no size overlap between the two kinds of magnetic beads. During the operation, the aggregation of both kinds of magnetic beads is not observed under the 20× microscope. The magnetic core in both beads was ferrite. According to the literature, the M-270 bead has magnetic content of 20 % and the MyOne beads have magnetic content of 37 % (Yellen et al. 2007). In both cases, the magnetic content is measured in volume percentage. During operation, the magnetic beads were placed in a droplet. The magnetic beads are added into the DI water by a dilution factor of 200, which leaves the concentration of magnetic beads to be 1×10^7/ml. DI water droplets were surrounded by 2cSt silicone oil filling the channel during operation in order to prevent droplet evaporation.

3.3.2 Experiment set-up

The experimental set-up consisted of four parts: observation microscope, connection stage, EWD function controller and magnetic function controller. The experiment could be viewed using a microscope through the top plate of the chip. The chip was placed on a CNC machined aluminium connection stage, where the connection between both controllers and the chip was made through a pair of clips. The detailed picture of the connection stage is shown in Fig. 5B. The control system for the EWD function requires a power supply providing the EWD actuation voltage and a switching circuit for voltage distribution. The switching signal was generated by the controlling computer and passed down to the control PCB. The whole controlling set-up for the EWD function is shown in Fig. 5C. The magnetic function controlling system consisted of a power source to supply the current and the controlling PCB. The controlling signal is generated by the same computer controlling the EWD function. The entire system is shown in Fig. 5C.

3.3.3 Magnetic bead segregation experiments

The first experiment was designed to study magnetic bead transport. A total of six sets of experiments were conducted to verify beads' movement in different combinations of magnetic beads and wire current. Both the 1- and 2.8-μm magnetic beads were used in those experiments; movement of each bead was studied under three different current conditions. The magnitude of the current was within the range from 100 to 300 mA. In all six experiments, magnetic beads were moved from one current wire to the next in a direction perpendicular to the wire. The total time for magnetic beads to travel between adjacent wires under different current conditions was recorded.

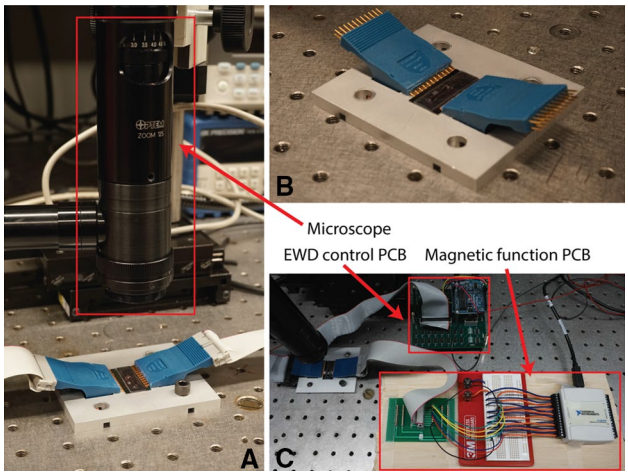

Fig. 5 *A* The observation microscope was placed above the testing stage, and the chip was placed on the testing stage and clipped in place. *B* A close-up picture of the connection stage. *C* The entire system is shown including the EWD controller and the magnetic function controller. The PCB in the upper part of the picture is the EWD controller, which can control up to 32 channels. The *lower part* of the picture shows the magnetic function controller, which sits on a wooden board. The controller is used to control seven current wires on the chip independently

The second experiment explored magnetic bead segregation in conjunction with droplet splitting. The experimental procedure started with dispensing a droplet containing magnetic beads. Then the droplet was actuated along the string of EWD electrodes to the electrode with integrated current wires. During bead segregation, the magnetic beads were collected to the location of the leftmost current wire. To collect the magnetic beads, currents were sequentially passed through all seven wires from right to the left. The segregation efficiency was recorded in all three cases with different wire spacing. After bead collection at the left side of the droplet, the droplet was then split, resulting in two daughter droplets. One of the daughter droplets contained the majority of magnetic beads, and the other droplet contained only DI water and unresponsive beads.

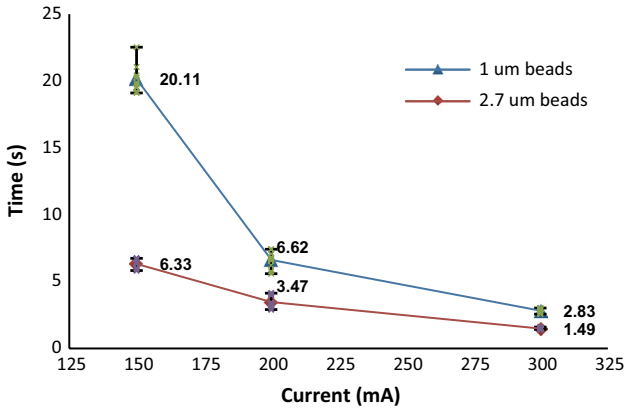

Fig. 6 Average times required for 1-μm (*triangle*) and 2.8-μm (*diamond*) magnetic beads to travel 65 μm under different current conditions. The *blue line* indicates the time needed for 1-μm beads to travel 65 μm. The *error bars* indicate the maximum and minimum time values in the ten experiments conducted at each current. The *blue line* represents the 2.8-μm beads, and the *error bar* indicates the maximum and minimum value from a total of six experiments under each condition. Each experiment is indicated in the figure by (×) (colour figure online)

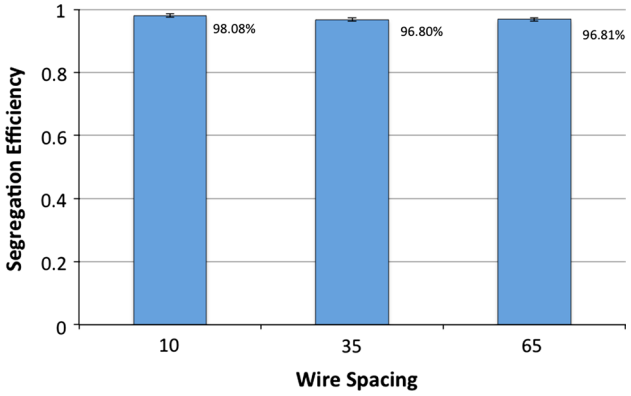

Fig. 7 Segregation efficiency is shown in this graph. The magnetic beads used in this experiment were 2.8-μm beads. The data points shown represent the average segregation efficiency from a total of five experiments conducted for each wire spacing

3.3.4 Magnetic beads separation experiments

The separation of magnetic beads by size was explored using two sizes of beads within the same droplet. The experiment started by initially placing both 2.8- and 1-μm-sized beads in a droplet over the same wire, passing a current through an adjacent wire, and then attempting to actuate the beads. Due to the difference in the magnetic moments between the two kinds of beads when the magnetic field is created, it was expected that the time required for 2.8-μm magnetic beads to cross the wire spacing would be less than that for the 1-μm beads, thus causing bead separation by size.

4 Results

The first experiment focused on the magnetic beads' response to different current conditions. Two things needed to be studied in this experiment: the consistency of bead response when exposed to a given magnetic field and the time required for the magnetic beads to move from one wire to the next. The resulting measurements are shown in Fig. 6. The horizontal axis is the wire current, and the vertical axis is the time required for beads to travel laterally 65 μm between wires. The time required by both types of magnetic beads to cross the wire spacing decreased as the current increased due to increased magnetic force with increasing field. When the current was 150 mA, it takes an average time of 20 s for the 1-μm magnetic beads to travel 65 μm between two wires. There were a total of 10 data points used to get the average time of flight at each value of current.

The average transit times for the 2.8-μm beads are also shown in Fig. 6. The error bars indicate the spread in times over six experiments at each current. When the current was 150 mA, it took an average time of 6.3 s for the 2.8-μm magnetic beads to travel 65 μm between two wires. The time of flight decreased as the current increased. Comparing the time of flight of 1- and 2.8-μm magnetic beads under the same current conditions, it is obvious that the 2.8-μm bead transit time was shorter for all currents used. The amount of magnetic content inside the two different kinds of beads explains the difference in the time of flight.

The results in Fig. 6 indicate that when the wire current was low, the two kinds of beads had the largest difference in transit times. As the wire current increased, the time difference decreased; hence the separation effect will diminish as well. The best separation among three conditions occurred in the 150 mA case where the time difference between the two kinds of beads was about 13.7 s. As shown later in this section, the separation experiments were conducted in the low-current condition.

The second experiment focused on the segregation efficiency of the device. Initially, the magnetic beads were uniformly dispersed within the droplet. The wire current was then passed sequentially through all the wires from right to the left, one by one. By moving the current from one wire to the next, magnetic bead l follows the movement of the magnetic field peak. As a result, the beads originally dispersed within the droplet were collected by each wire and transported to the leftmost wire. The result of this segregation is shown in Fig. 7, indicating the percentage of magnetic beads that were concentrated onto the leftmost current wire in three different wire spacing devices. The segregation result

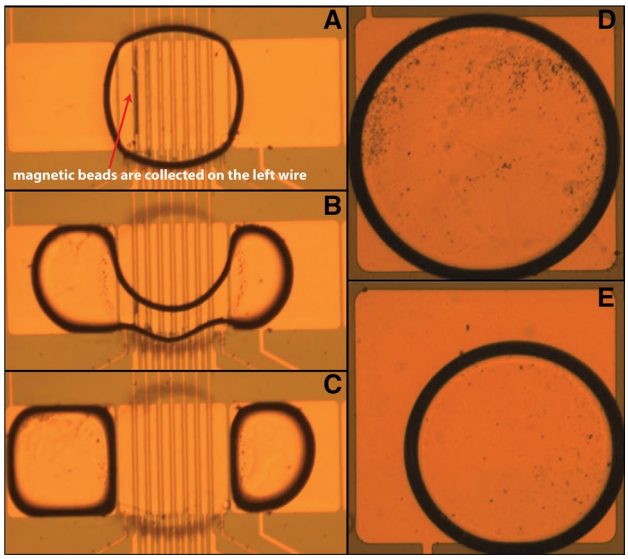

Fig. 8 *A* Magnetic beads were collected to the *left*most wire's location. *B* The droplet is split into two sub-droplets, while the magnetic function is still active to ensure the magnetic beads stay in the *left-hand* droplet. *C* The droplet was split. *D* An *enlarged image* of the *left* sub-droplet showing the majority of magnetic beads inside. *E* An *enlarged image* showing the *right* sub-droplet

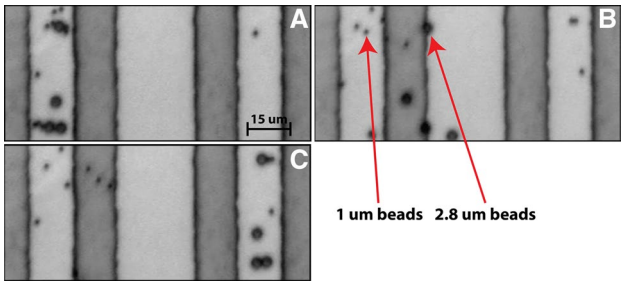

Fig. 9 *A* Both 1- and 2.8-μm magnetic beads were collected on the *left* current wire. This wire was the starting point for the experiment. *B* The current was applied in the *right*most current wire 65 μm away. The 2.8-μm-diameter magnetic beads were attracted to the wire on the *right*. At this stage of the movement, the *larger* beads have moved further compared with the 1-μm beads. *C* The 2.8-μm beads have been collected onto the location of the *right*most current wire, while the 1-μm beads are still 40 μm away from the wire's location. Separation of the two kinds of beads is achieved within 65-μm distance

shows that all three cases achieve high segregation efficiency above 96 %. The differences in the three cases were the current control patterns chosen to achieve the segregation efficiency. The first case used devices with wire spacing of 10 μm. In this case, the current in each wire is 200 mA, and current was applied in each wire for 2 s in a single pass. In the second case, the device had wire spacing of 35 μm. In order to achieve high segregation efficiency, the current needed to be turned on for 4 s in each wire. The current was 200 mA, and it was sequenced through the wires only once. Similarly when the wire spacing was 65 μm, the current was turned on sequentially for 16 s in each wire. However, high segregation efficiency was only achieved after four passes of currents through the wires. It can be seen from the experiment that the smaller the distance between wires, the easier it was for the magnetic beads to be segregated. However, regardless of the current control pattern, high segregation efficiency could be achieved.

Droplet splitting was used to complete bead segregation. The leftmost current wire was placed close to the left edge of the electrode. When droplet splitting action occurred, the current in the leftmost wire was kept on and the magnetic beads were held in that location. Figure 8A–C illustrates droplet splitting, while the beads were kept stationary by the current in the leftmost current wire. Figure 8D, E shows the resulting two droplets. It is clear that the droplet on the left has a much higher concentration of magnetic beads compared with the droplet on the right.

The third experiment demonstrated that two kinds of magnetic beads can be separated within a droplet. As it was shown in the first experiment that the 1- and 2.8-μm-diameter magnetic beads react differently to 150 mA wire currents. The difference in time of flight can be used as a way to separate beads within the distance of 65 μm. As shown in Fig. 9A, two wires were located on either side of the photograph. Both kinds of beads were located in a droplet over the left current wire. This was achieved by applying current in the left wire. After the beads were collected to that wire, 150 mA of current was then switched on in the rightmost wire 65 μm away. Due to the difference in magnetic content inside the two kinds of beads, the 2.8-μm beads moved faster than the 1-μm beads, as shown in Fig. 9B. After all the 2.8-μm beads were collected to the position of the rightmost wire, the smaller diameter beads were still in close vicinity to the left wire. The average distance between the two sets of beads was about 40 μm, as shown in Fig. 9C. The total time to achieve this result was <10 s.

5 Discussion

The experiments designed and conducted were aimed at gaining more complex intra-droplet control of magnetic beads compared to bead control using a permanent magnet. Many factors were considered when controlling beads with finer precision using current wires, such as the beads' magnetic content, the beads' diameter, the current wire spacing, the geometry of the wires, current magnitude and its switching pattern. The first experiment used different wire currents to determine the average transit times required by different beads. The magnetic beads' movement in these

experiments was accelerated movement from a stationary position. The accelerated motion occurred, since the magnetic moment of the beads and the magnetic field gradient increased as the magnetic beads moved closer to the current wire. The results of the experiments show a clear trend that less time is required by the magnetic beads to travel a certain distance when the current and magnetic content inside the beads are higher. At low wire currents, the difference in time of flight between 1- and 2.8-μm beads was largest. Hence, the low-current condition is better suited for best bead separation. The experiments also confirm that using a current wire structure to control magnetic beads can result in adequate consistency. Such consistency is useful in many other experiments such as segregation and separation as discussed next.

The second experiment demonstrated the segregation efficiency in conjunction with droplet splitting. The segregation effect was studied using different wire spacing. According to theory, it is expected that larger wire spacing will result in a longer segregation process. This is reflected by the time that the current needs to be turned on in order to achieve high segregation efficiency. In the case where the wire spacing was 65 μm, the wire current needed to be turned on for 16 s in each wire, and it required four passes to achieve 96 % segregation efficiency. Although the current control pattern in each case was different, high segregation efficiency was achieved in all three cases.

Droplet actuation was demonstrated on an electrode with integrated current wires. The droplet splitting after segregation is a useful tool for magnetic bead concentration and washing. The experiment successfully split a droplet after segregation was completed, resulting in two daughter droplets with significantly different bead concentrations. The splitting of the droplet after segregation is the only one example demonstrated to show the capability of the device. The potential of the device comes from the fact that the magnetic bead control function and the EWD function can be operated independently and simultaneously. The reason for this is the voltage supplied by the EWD electrode has a very small effect on the magnetic beads (induces small convection currents in the liquid) relative to the magnetic forces created by the current wires. In addition, the current wires only require voltages at least one order of magnitude smaller than the EWD actuation voltage. The EWD actuation voltage does not significantly affect the movement of the magnetic beads, and droplet actuation is not being affected by the low voltage applied to drive currents through the wires. Such characteristics of the device allow great possibilities for all kinds of operations; any combination of the magnetic function and the EWD function can be explored. This will give great flexibility when designing experimental protocols.

The third experiment was a confirmation of using the current wires to perform magnetic bead separation. The result demonstrated that the 1- and 2.8-μm beads could be separated within the spacing of two adjacent wires. In the experiment, the wire spacing was 65 μm and the distance between the two kinds of beads after separation was 40 μm. This experiment showed the feasibility of performing separation in droplets with a complex mixture of multiple beads, each having different magnetic contents. With multiple wires in the device, the separation across the whole droplet can be achieved by performing sequential small separations between adjacent pairs of wires. The experiment is shown to use magnetic beads only to access the performance of the device. Although the purpose of this paper is to show the performance of the device, it is also beneficial to discuss about the performance change due to bio-samples attached to magnetic beads. Assuming the current conditions stay the same, the factors that influence the speed of the magnetic beads are the magnetic content, total volume of the beads and the shape of the magnetic beads. When the bio-samples attach to the magnetic beads, the magnetic content percentage decreases and the size increases as the bio-sample and magnetic beads considered as a whole. Those changes will decrease the speed of the particle movement. When the samples are proteins, its size is small compared to the magnetic beads; hence, the performance of the particle will not change by much. When the sample is cells, which is usually comparable to the size of magnetic beads, the speed of the particles is expected to be slower. Regardless of the performance change due to the bio-samples, the segregation efficiency discussed in experiment one should not change.

During all the experiments conducted, the chip was mounted on a stage, where the connection of the chip and the controller was via clips, as shown in Fig. 5. The joule heat due to the current used in the system was small; hence, no damage to the device was observed nor was there any interference with device performance. The minimal amount of generated heat was dissipated through the metal stage. As a result, the device required no additional supporting systems other than the controller. The fabrication process of the device was exactly the same as typical EWD devices.

6 Conclusion

This paper demonstrates an EWD device with integrated current wires for magnetic bead control. The device uses parallel current wires as electromagnets to generate magnetic forces on the beads. This method is shown to have many advantages over previous systems. Compared with previous systems that operate with permanent magnets, the device shown in this paper does not require a mechanical

supporting system, which makes system integration easier. In addition, current wires allow for higher-resolution control of the magnetic beads. The current device's stack structure is identical to that of a normal EWD device, so integration does not require additional steps in the fabrication process of EWD devices.

Three experiments were conducted in this paper. The first experiment studied the different transit times required by different beads to travel 65 μm using several wire currents. The second experiment demonstrated the segregation of magnetic beads. In this experiment, high segregation efficiency was shown under different wire spacing conditions. This experiment also included the splitting of the droplet to form fully separated beaded and unbeaded droplets. The third experiment was used to demonstrate the possibility of separating at least two kinds of magnetic beads within a short distance. It was shown in the experiment that by using 150 mA of current, the 1- and 2.8-μm beads could be separated over 65 μm of distance in under 10 s.

The three experiments show the magnetic function in this device has high-resolution control over magnetic beads, and the magnetic beads can be segregated with high efficiency. The magnetic function requires a little off-chip support and can be easily integrated with an EWD system. Both the magnetic function and the EWD function can be operated simultaneously, and there is no discernible interference between them. Such a unique capability opens up additional possibilities in on-chip biological analysis protocols and provides future integration potential for other functions into a more capable system.

Acknowledgments This work was supported in part by the National Science Foundation under grant NSF-CNS-11-35853.

References

Alexiou C, Diehl D, Henninger P, Iro H, Röckelein R, Schmidt W, Weber H (2006) A high field gradient magnet for magnetic drug targeting. IEEE Trans Appl Supercond 16(2):1527

Arya SK, Lim B, Rahman AR (2013) Enrichment, detection and clinical significance of circulating tumor cells. Lab Chip 13(11):1995–2027

Berry SM, Alarid ET, Beebe DJ (2011) One-step purification of nucleic acid for gene expression analysis via Immiscible Filtration Assisted by Surface Tension (IFAST). Lab Chip 11(10):1747–1753

Boles DJ, Benton JL, Siew GJ, Levy MH, Thwar PK, Sandahl MA, Rouse JL, Perkins LC, Sudarsan AP, Jalili R, Pamula VK, Srinivasan V, Fair RB, Griffin PB, Eckhardt AE, Pollack MG (2011) Droplet-based pyrosequencing using digital microfluidics. Anal Chem 83(22):8439–8447

Chen LA, Madison and Fair RB (2014) Intra-droplet magnetic bead manipulation on a digital microfluidic chip. In: MicroTAS 2014. San Antonio

Cho SK, Zhao Y, Kim CJ (2007a) Concentration and binary separation of micro particles for droplet-based digital microfluidics. Lab Chip 7(4):490–498

Cho YK, Lee JG, Park JM, Lee BS, Lee Y, Ko C (2007b) One-step pathogen specific DNA extraction from whole blood on a centrifugal microfluidic device. Lab Chip 7(5):565–573

Fair RB (2007) Digital microfluidics: is a true lab-on-a-chip possible? Microfluid Nanofluid 3(3):245–281

Fair RB, Khlystov A, Tailor TD, Ivanov V, Evans RD, Griffin PB, Vijay S, Pamula VK, Pollack MG, Zhou J (2007) Chemical and biological applications of digital-microfluidic devices. Des Test Comput IEEE 24(1):10–24

Fonnum G, Johansson C, Molteberg A, Mørup S, Aksnes E (2005) Characterisation of Dynabeads® by magnetization measurements and Mössbauer spectroscopy. J Magn Magn Mater 293(1):41–47

Gao L, Gottron NJ 3rd, Virgin LN, Yellen BB (2010) The synchronization of superparamagnetic beads driven by a micro-magnetic ratchet. Lab Chip 10(16):2108–2114

Gijs MAM, Lacharme F, Lehmann U (2010) Microfluidic applications of magnetic particles for biological analysis and catalysis. Chem Rev 110(3):1518–1563

Grant IS, Phillips WR (2008) Electromagnetism, 2nd edn., Manchester Physics, Wiley, New York

Gupta AK, Gupta M (2005) Synthesis and surface engineering of iron oxide nanoparticles for biomedical applications. Biomaterials 26(18):3995–4021

He J, Huang M, Wang D, Zhang Z, Li G (2014) Magnetic separation techniques in sample preparation for biological analysis: a review. J Pharm Biomed Anal 101:84–101

Hiptmair R (2002) Finite elements in computational electromagnetism. Acta Numerica 11:237–339

Jones DS (2013) The theory of electromagnetism. Elsevier, Amsterdam

Lee CS, Lee H, Westervelt RM (2001) Microelectromagnets for the control of magnetic nanoparticles. Appl Phys Lett 79(20):3308

Lee H, Westervelt RM, Purdon AM (2004) Micromanipulation of biological systems with microelectromagnets. IEEE Trans Magn 40(4):2991

Mach AJ, Adeyiga OB, Di Carlo D (2013) Microfluidic sample preparation for diagnostic cytopathology. Lab Chip 13(6):1011–1026

Miller E, Wheeler A (2009) Digital bioanalysis. Anal Bioanal Chem 393(2):419–426

Mugele F, Baret J-C (2005) Electrowetting: from basics to applications. J Phys Condens Matter 17(28):R705

Pamme N, Wilhelm C (2006) Continuous sorting of magnetic cells via on-chip free-flow magnetophoresis. Lab Chip 6(8):974–980

Shah GJ, Veale JL, Korin Y, Reed EF, Gritsch HA, Kim CJ (2010) Specific binding and magnetic concentration of CD8+ T-lymphocytes on electrowetting-on-dielectric platform. Biomicrofluidics 4(4):44106

Sista RS, Eckhardt AE, Srinivasan V, Pollack MG, Palanki S, Pamula VK (2008) Heterogeneous immunoassays using magnetic beads on a digital microfluidic platform. Lab Chip 8(12):2188–2196

Sung Kwon C, Chang-Jin K (2003) Particle separation and concentration control for digital microfluidic systems. In: Micro electro mechanical systems, 2003. MEMS-03 Kyoto. IEEE the sixteenth annual international conference on

Tao J, Cheung NW, Hu C (1993) Electromigration characteristics of copper interconnects. IEEE Electron Device Lett 14(5):249

Walker SW, Shapiro B, Nochetto RH (2009) Electrowetting with contact line pinning: computational modeling and comparisons with experiments. Phys Fluids (1994-present) 21(10):102103

Welch ERF, Lin Y-Y, Madison A, Fair RB (2011) Picoliter DNA sequencing chemistry on an electrowetting-based digital microfluidic platform. Biotechnol J 6(2):165–176

Wirix-Speetjens R, Boeck Jd (2004) On-chip magnetic particle transport by alternating magnetic field gradients. IEEE Trans Magn 40(4):1944–1946

Wognum AW, Eaves AC, Thomas TE (2003) Identification and isolation of hematopoietic stem cells. Arch Med Res 34(6):461–475

Yellen BB, Erb RM, Son HS, Hewlin R Jr, Shang H, Lee GU (2007) Traveling wave magnetophoresis for high resolution chip based separations. Lab Chip 7(12):1681–1688

Zhang Y, Wang TH (2013) Full-range magnetic manipulation of droplets via surface energy traps enables complex bioassays. Adv Mater 25(21):2903–2908